Strain-induced chiral magnetic effect in Weyl semimetals

Alberto Cortijo, Dmitri Kharzeev, Karl Landsteiner, and Maria A. H. Vozmediano

Phys. Rev. B **94**, 241405 — Published 19 December 2016

DOI: 10.1103/PhysRevB.94.241405

Strain induced Chiral Magnetic Effect in Weyl semimetals

Alberto Cortijo[1], Dmitri Kharzeev[2,3], Karl Landsteiner[4] and Maria A.H. Vozmediano[1]

[1] *Instituto de Ciencia de Materiales de Madrid, C/ Sor Juana Inés de la Cruz 3, Cantoblanco, 28049 Madrid, Spain*

[2] *Department of Physics and Astronomy, Stony Brook University, Stony Brook, New York 11794-3800, USA*

[3] *Department of Physics and RIKEN-BNL Research Center, Brookhaven National Laboratory, Upton, New York 11973-5000, USA*

[4] *Instituto de Física Teórica UAM/CSIC, C/ Nicolás Cabrera 13-15, Cantoblanco, 28049 Madrid, Spain*

We argue that strain applied to a time-reversal and inversion breaking Weyl semi-metal in a magnetic field can induce an electric current via the chiral magnetic effect. A tight binding model is used to show that strain generically changes the locations in the Brillouin zone but also the energies of the band touching points (tips of the Weyl cones). Since axial charge in a Weyl semi–metal can relax via inter-valley scattering processes the induced current will decay with a timescale given by the lifetime of a chiral quasiparticle. We estimate the strength and lifetime of the current for typical material parameters and find that it should be experimentally observable.

I. INTRODUCTION

Chiral anomalies belong to the most emblematic predictions of quantum field theory[1]. In the presence of massless (chiral) fermions not all the symmetries of the classical theory are compatible with the quantum theory. The theory of anomalies has a very wide range of applications reaching from particle physics to condensed matter physics. In the recent years anomaly induced transport phenomena, such as the chiral magnetic effect (CME) have attracted much attention in the quark–gluon plasma[2–4], and in Dirac matter[5,6]. The recently synthesized Weyl semimetals (WSM)[7–9] are an optimum benchmark to test anomaly related phenomena in condensed matter. These materials have chiral Weyl points separated in momentum space. The minimal model with two Weyl nodes in a continuum description is described by the action

$$S = \int d^4k \bar{\psi}_{-k}(\gamma^\mu k_\mu - m - b_\mu \gamma^\mu \gamma_5)\psi_k. \qquad (1)$$

which resembles a Lorentz breaking QED action[10,11]. The WSM phase is reached when the parameters obey the condition $-b^2 > m^2$ in which case the separation between nodes is proportional to the four-vector $\Delta k^\mu \equiv \lambda^\mu \sim b^\mu \sqrt{1 - \frac{m^2}{b^2}}$.

The CME describes the generation of an electric current parallel to an applied magnetic field in chirally imbalanced matter[2–4]. It the context of Weyl semi-metals it is best described by the formula[5,12]

$$\vec{J} = \frac{\mu_L - \mu_R + E_L - E_R}{4\pi^2}\vec{B} = \frac{\mu_5 - \lambda_0}{2\pi^2}\vec{B}\,, \qquad (2)$$

where $\mu_{L,R}$ are the chemical potentials of left- and right-handed fermions as measured from the tips of the Weyl cones whereas $E_{L,R}$ are the energies at which the Weyl cones are located. The axial chemical potential is $2\mu_5 = \mu_L - \mu_R$ and the difference in energy of the band touching points is $2\lambda_0 = E_R - E_L$.

The axial symmetry is not exact. It is broken even at tree level by the mass term in (1). In a crystal this is unavoidable due to the compactness of the Brillouin zones. Therefore axial charge will decay to a thermodynamic equilibrium state in which the left- and right-handed fermi surfaces sit at the same energy such that $E_L + \mu_L = E_R + \mu_R$. The CME vanishes in a Weyl semi-metal in thermodynamic equilibrium[5,11].

In order to induce a non-vanishing chiral magnetic current it is clear from (2) that there are in principle two options. First one might modify the chemical potentials by inducing an imbalance in the occupation numbers of left- and right-handed fermions. One way to do this is to use the proper axial anomaly

$$\partial_\mu J_5^\mu = \frac{1}{2\pi^2}\vec{E}\cdot\vec{B}\,. \qquad (3)$$

In parallel electric and magnetic fields, fermions are pumped via spectral flow from one Weyl-cone to the other and thereby changing their chirality. This process leads to a dramatic enhancement of the electric conductivity along the direction of the magnetic field. The anomaly induced negative magnetoresitivity has indeed been verified experimentally in Dirac and Weyl semi-metals[13–16].

A second possibility is to change the locations of the Weyl cones $E_{L,R}$. We argue in the reminder of this work that this can indeed be achieved by applying strain, in particular, it will be induced by the time component of the axial elastic vector field that emerges when lattice deformations are included in the model. As a result, we find an elastic contribution to the chiral magnetic effect linearly proportional to the strain tensor u_{ij} and to the Grüneisen parameter of the material β.

II. STRAIN INDUCED CHIRAL IMBALANCE

The local band structure for a WSM with two Weyl points is described by the continuum model

$$S = \int d^4k \bar{\psi}_k(\gamma^\mu k_\mu - \lambda_\mu \gamma^\mu \gamma_5)\psi_k. \qquad (4)$$

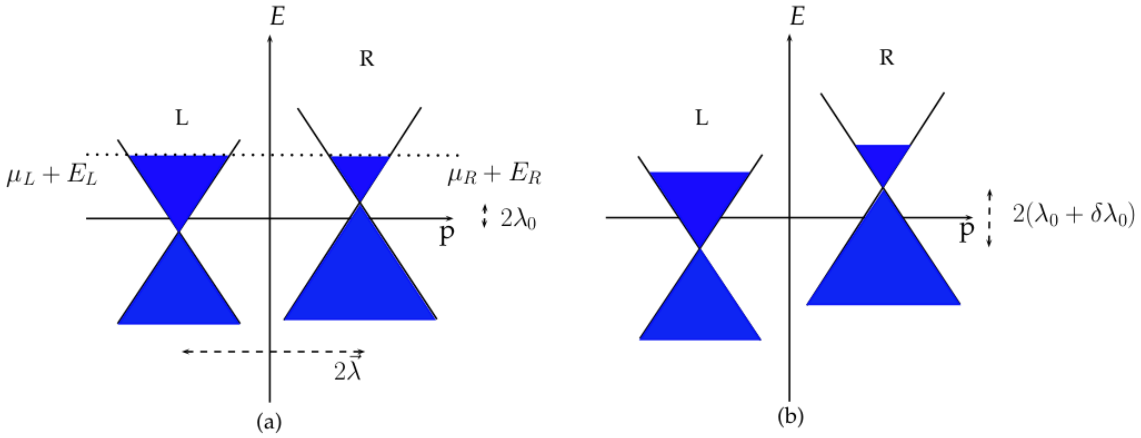

FIG. 1. (Color online) Local band structure of a Weyl semimetal with two nodal points at different energies and different position in momentum space. In (a) there are Fermi surfaces of different sizes for left- and right-handed fermions as measured by the left- and right-handed chemical potentials $\mu_{L,R}$. The Fermi energy of both Weyl cones is however the same in equilibrium resulting in vanishing CME. In (b) the situation shortly after applying strain is depicted. The tips of the Weyl cones have shifted in energy but the Fermi surfaces have not yet had enough time time to equilibrate $t < \tau_{\rm inter}$. The CME is given by $\vec{J} = \frac{\delta\mu_5(t) - \delta b_0}{2\pi^2}\vec{B}$. Over a timescale given by the inter valley scattering time $\tau_{\rm inter}$ the axial chemical potential $\delta\mu_5$ will build up such at for for $t \gg \tau_{\rm inter}$ it takes the value $\delta\mu_5 = \delta b_0$ and equilibrium with vanishing CME is reached again.

The schematic band structure is represented in Fig. 1. The space components of the vector λ_μ break time reversal symmetry and its magnitude sets the separation of the Weyl nodes in momentum space. Its time component λ_0 breaks inversion symmetry and marks the separation in energy of the points. The emergence of elastic gauge fields coupling with opposite signs to the two chiralities (axial) in time reversal breaking Weyl semimetals was derived from a tight binding model in ref. (17) (see also (18)). But, as we discussed earlier, the chiral magnetic effect requires a time component of the elastic gauge field not described before in graphene or in any other material. In what follows we will give the main lines of the derivation of the time component for the elastic gauge field. A full detail of this derivation is provided in the supplemental material.

A tight binding model that captures the physics of a WSM containing a pair of Weyl nodes separated both in energy and in momentum space is described by the Hamiltonian

$$H_0 = \sum_{\boldsymbol{k},s} t\sin(k_s a) c^+_{\boldsymbol{k}} \alpha_s c_{\boldsymbol{k}} - r\sum_{\boldsymbol{k},s}\cos(k_s a) c^+_{\boldsymbol{k}}\hat{\beta} c_{\boldsymbol{k}} + \quad (5)$$
$$+ \Delta\sum_{\boldsymbol{k}} c^+_{\boldsymbol{k}}\hat{\beta} c_{\boldsymbol{k}} + b_3\sum_{\boldsymbol{k}} c^+_{\boldsymbol{k}}\alpha_3\gamma_5 c_{\boldsymbol{k}} + b_0\sum_{\boldsymbol{k}} c^+_{\boldsymbol{k}}\gamma_5 c_{\boldsymbol{k}}.$$

A detailed description of this Hamiltonian is given in Section A. The last term in (6) accounts for a relative energy shift of the energies of the Weyl points. The effect of the elastic deformations can be taken into account by knowing how the hopping parameters t, and r change under strain[19]:

$$t\alpha_s \to t(1-\beta u_{ss})\alpha_s + t\beta\sum_{s'\neq s} u_{ss'}\alpha_{s'}, \qquad (6a)$$

$$r \to r_s = r(1-\beta u_{ss}). \qquad (6b)$$

Inserting these changes in (6), and expanding around the Weyl nodes, we obtain the part of the Hamiltonian that depends on the strain:

$$H[u] = \sum_k \left(2\tau b_0\beta\frac{v\lambda_3}{m+b_3}u_{33}\right)\psi^+_{\boldsymbol{k}}\sigma_0\psi_{\boldsymbol{k}} +$$
$$+ \sum_{k,s=1,2}\left(\tau\beta v\lambda_3 u_{3s}\right)\psi^+_{\boldsymbol{k}}\sigma_s\psi_{\boldsymbol{k}} +$$
$$+ \sum_k\left(2\beta\frac{v^2\lambda_3^2}{m+b_3}u_{33} - \beta r Tr[u]\right)\psi^+_{\boldsymbol{k}}\sigma_3\psi_{\boldsymbol{k}}, \quad (7)$$

where $\tau = \pm 1$ labels the chirality of each Weyl node. The last two terms were derived previously[17], while the first term is the *temporal* component of the elastic vector field. The same derivation can be obtained from general symmetry arguments along the lines of ref.[20]. We note that, from a general symmetry approach, even if the unstrained material has $b_0 = 0$, an effective coupling of the form $\tau A_0(x)\sigma_0$ will be generated in the low energy effective action since a generic strain deformation will break inversion symmetry. Moreover, since rotational invariance is broken in the material by the vector $\mathbf{b}$, the only symmetry remaining is rotations in the perpendicular plane. If $\mathbf{b}$ points, say, along the OZ axis, the u_{33} component of the strain tensor is a scalar quantity that can be coupled to any term in the effective Hamiltonian.

This part of the elastic gauge field shifts the locations of the Weyl points when elastic deformations are induced in the system and induce an effective axial gauge field:

$$2(\delta\lambda_0) = (E_L - E_R)\beta u_{33}\,. \qquad (8)$$

The strain induced CME is proportional to the difference in energies of the Weyl-cones before applying strain, to the Grüneisen parameter of the material, and to the magnitude of the strain itself. Since eventually the Fermi surfaces will equilibrate by processes such as inter–valley scattering or through spectral flow through the edge states (Fermi arcs), this strain induced CME will be observable only over a short timespan set by the lifetime $\tau_{\rm inter}$ of a chiral quasiparticle at the corresponding Fermi surface. This time is estimated to be much larger than the intra-valley scattering rate or the usual impurity induced lifetime[21,22]. Taking anomaly and inter–valley scattering into account the time developement of the axial chemical potential is given by

$$\partial_t \rho_5 = \frac{1}{2\pi^2}\vec{E}\cdot\vec{B} - \frac{1}{\tau_{\rm inter}}\left(\rho_5 - \rho_5^{(eq)}\right) \qquad (9)$$

where $\rho_5^{(eq)} = \rho_5(\lambda_0 + \delta\lambda_0)$. The relation between the axial chemical potential and the axial charge is given by the equation of state $\rho_5 = \frac{\partial P}{\partial \mu_5}$ with P the the thermodynamic pressure for chiral fermions. This will result in an exponentially decaying strain induced chiral magnetic current

$$\vec{J} = \frac{\delta\lambda_0}{2\pi^2}\vec{B}e^{-t/\tau_{\rm inter}} = \frac{(E_L - E_R)\beta u_{33}}{4\pi^2}\vec{B}e^{-t/\tau_{\rm inter}}\,. \quad (10)$$

III. PHYSICAL FEASIBILITY OF THE PROPOSAL

We can estimate the strength of the current by taking the typical separation of the Weyl nodes in energy be of the order of 1 meV, the Grüneisen parameter $\beta = 1$ and the attainable amount of strain in the percentage realm (1%). The resulting current is

$$\vec{J} \approx 10^5 \cdot \vec{B}\ [A/m^2], \qquad (11)$$

with the magnetic field B expressed in Tesla. For a sample of a cross section of $10\mu m^2$ the induced current is of the order of 10 microamperes in a magnetic field of 1T[23]. This an observable quantity of the same order of magnitude as the one described in[24,25]. Since the considered WSM materials break inversion symmetry, they will also be piezoelectric. For comparison, the maximum current in a typical piezoelectric varies from nA to μA and the voltage generated in $1-100V$, depending on the size of the material. The CME signal should be easily distinguishable from the standard piezo response due to its linear dependence on the magnetic field. The current will decay exponentially within a typical time $10\tau_{inter}$.

For the expression (2) to be applicable we need to assume that the strain induced deformation acts on a time scale which is slow compared to the equilibration time with a Weyl cones but faster than the equilibration time for the axial charge, i.e. the inter valley scattering time. This can be fulfilled in WSM where inter valley relaxation time is estimated to be at least two orders of magnitude larger than standard lifetime[21].

A potential difficulty to measure the effect lies on the fact that the inter-valley relaxation time (estimated to be of the order of 10^{-9} s at best[22]) is of the same order of magnitude than the time needed for the elastic perturbation to propagate along the sample (assumed of microns size) what might attenuate the signal. Still the magnitude of the induced current will be within the observable range.

Time reversal symmetry breaking Weyl semimetals (both type-I and type-II) have been experimentally reported recently[26,27], while others have been theoretically proposed[28,29]. It is thus expected that the present proposal can be tested in the near future. Anomaly related transport phenomena in WSM[11,30–32] and effects of strain in WSM[33,34] have been considered previously in various contexts but the contribution of elastic gauge fields is novel and potentially more relevant. Another interesting possibility is that elastic gauge fields could realize the Topological Lifshitz transitions described in[3536].

Note added: After completion of this manuscript two works appeared in the arXiv[37,38] concerning the effect of strain on WSM. These works rely on the elastic gauge fields deduced in ref.[17] that only had spatial components. The chiral magnetic effect presented in this work is an entirely new contribution based on the time component of the elastic gauge field derived in the appendix that has not been described before neither in the WSM nor in graphene.

ACKNOWLEDGMENTS

MAHV thanks F. de Juan and A. Grushin for useful conversations. The work of A. C. and M.A.H.V. has been supported by Spanish MECD grants FIS2014-57432-P, the European Union structural funds and the Comunidad de Madrid MAD2D-CM Program (S2013/MIT-3007), the MINECO (Spain) Grant No. FIS2015-73454-JIN, and by the European Union Seventh Framework Programme under grant agreement no. 604391 Graphene Flagship. The work of D. K. has been supported by in part by the U.S. Department of Energy under Contracts No. DE-FG- 88ER40388 and DE-AC02-98CH10886. The work of K.L. has been supported by Severo Ochoa Programme grant SEV-2012-0249 and by FPA2015-65480-P (MINECO). K.L. and M.A.H.V. gratefully acknowledge support from the Simons Center for Geometry and Physics, Stony Brook University at which some of the research for this paper was performed.

Appendix A: Time component of the elastic gauge field

1. The model with b_0

The minimal tight binding model reproducing the band structure of WSM is that of of s-, and p-like electrons hopping in a cubic lattice and chirally coupled to an on-site constant vector field b_μ[11,19]:

$$H_0 = \sum_i \sum_s \frac{-1}{2} c_i^+ \left(r\hat{\beta} + it\alpha_s \right) c_{i+s} - \frac{1}{2} c_{i+s}^+ \left(r\hat{\beta} - it\alpha_s \right) c_i + \sum_i \Delta \; c_i^+ \hat{\beta} c_i \\ + \sum_i b_3 c_i^+ \alpha_3 \gamma_5 c_i + \sum_i b_0 c_i^+ \alpha_3 c_i, \tag{A1}$$

where t, r, m are hopping parameters between s and p states, hopping between the same kind of states, and the difference of on-site energies between s and p states, respectively. The parameter Δ is $\Delta = m + 3r$. Without loss of generality, we choose the vector field $\boldsymbol{b}$ to point along the OZ direction b_3. This spacial component breaks time reversal $\mathcal{T}$ and $SO(2)$ rotational symmetry; the time component b_0 shifts the Weyl cones in energy and breaks inversion symmetry. In momentum space,

$$H_0 = \sum_{\boldsymbol{k},s} t \sin(k_s a) c_{\boldsymbol{k}}^+ \alpha_s c_{\boldsymbol{k}} - r \sum_{\boldsymbol{k},s} \cos(k_s a) c_{\boldsymbol{k}}^+ \hat{\beta} c_{\boldsymbol{k}} + \Delta \sum_{\boldsymbol{k}} c_{\boldsymbol{k}}^+ \hat{\beta} c_{\boldsymbol{k}} + b_3 \sum_{\boldsymbol{k}} c_{\boldsymbol{k}}^+ \alpha_3 \gamma_5 c_{\boldsymbol{k}} + b_0 \sum_{\boldsymbol{k}} c_{\boldsymbol{k}}^+ \gamma_5 c_{\boldsymbol{k}}. \tag{A2}$$

with $s = 1, 2, 3$. We will use the following set of Dirac matrices, $\alpha_1 = \tau_0\sigma_1$, $\alpha_2 = \tau_0\sigma_2$, $\alpha_3 = \tau_1\sigma_3$, $\hat{\beta} = \tau_3\sigma_3$, $\gamma_5 = \tau_1\sigma_0$, so $\alpha_3\gamma_5 = \tau_0\sigma_3$.

We will choose to expand the Hamiltonian (A2) around the $\boldsymbol{k} = 0$ point ($\boldsymbol{k} \cdot \boldsymbol{p}$ theory) and compute the value of the emergent Fermi points within this approximation. When computing the effect of the strain we will start from this approximation. Around the Γ point, $\sin(k_s a) \simeq k_s a$, and $\cos(k_s a) \simeq 1$, so the Hamiltonian matrix reads ($v = ta$, and $m = \Delta - 3r$)

$$\mathcal{H}_0(\boldsymbol{k}) = \begin{pmatrix} v\boldsymbol{\sigma} \cdot \boldsymbol{k}_\perp + (m + b_3)\sigma_3 & vk_3\sigma_3 + b_0\sigma_0 \\ vk_3\sigma_3 + b_0\sigma_0 & v\boldsymbol{\sigma} \cdot \boldsymbol{k}_\perp + (b_3 - m)\sigma_3 \end{pmatrix}, \tag{A3}$$

acting on the spinor $\Psi_{\boldsymbol{k}} = (\phi_{\boldsymbol{k}}, \psi_{\boldsymbol{k}})^T$. The momentum $\boldsymbol{k}_\perp$ is the momentum perpendicular to b_3. The main difference with respect to the original case is that now, for energies $\omega, v|\boldsymbol{k}_\perp| \ll m + b_3$, the high energy sector represented by $\phi_{\boldsymbol{k}}$ is related to $\psi_{\boldsymbol{k}}$ through

$$\phi_{\boldsymbol{k}} \simeq -\frac{\sigma_0 v k_3 + \sigma_3 b_0}{m + b_3} \psi_{\boldsymbol{k}}, \tag{A4}$$

and the effective two-band model is

$$H_{eff} = \sum_{\boldsymbol{k}} \psi_{\boldsymbol{k}}^+ \left(-\frac{2b_0 v k_3}{m + b_3}\sigma_0 + v\boldsymbol{\sigma} \cdot \boldsymbol{k}_\perp + \frac{1}{m + b_3}(b_3^2 - b_0^2 - m^2 - v^2 k_3^2)\sigma_3 \right) \psi_{\boldsymbol{k}}. \tag{A5}$$

The presence of b_0 induces two differences: first, there is a term proportional to the identity matrix σ_0 and *linearly* dependent on k_3 breaking inversion symmetry (in the original full lattice model, it would be proportional to $\sin(k_3 a)$), and second, it modifies the mass term accompanying the σ_3 matrix.

The condition to obtain the Weyl nodes is now when the two bands intersect each other: $E_+(\boldsymbol{k}) = E_-(\boldsymbol{k})$, so the positions of the Weyl nodes change correspondingly to:

$$\lambda_\pm = \pm\lambda_3 = \pm\frac{\sqrt{b_3^2 - b_0^2 - m^2}}{v}, \tag{A6}$$

that is, when $b_0 = 0$, the two Weyl nodes appeared for values of $b_3 > m$. Now, the situation is a little bit more complex (and richer), since for some values of the three parameters m, b_3, and b_0 it might happen that the maximum of the valence band is placed at higher energies than the minimum of the conduction band, but the two bands do not intersect at any real momentum. The energies where the new Weyl nodes are placed read:

$$E_\pm = \mp 2b_0 \frac{\sqrt{b_3^2 - b_0^2 - m^2}}{m + b_3}. \tag{A7}$$

Expanding around λ_3, $k_3 = \pm\lambda_3 + \delta k_3$, for small δk_3 the Hamiltonian matrix around the two Fermi points take the form ($\tau = \pm 1$ labels the two Weyl points)

$$H^W_\tau(\boldsymbol{k}) = \tau \frac{2vb_0\lambda_3}{m+b_3}\sigma_0 + v\boldsymbol{\sigma}\cdot\boldsymbol{k}_\perp + \tau v_3(k_3+\tau\lambda_3)\sigma_3, \tag{A8}$$

that is, the Hamiltonian of two Weyl modes with opposite chirality $\left(v_3 = 2v\sqrt{\frac{b_3^2-b_0^2-m^2}{(b_3+m)^2}}\right)$.

2. Elastic deformations

Elastic deformations of the lattice induce the following two changes in the Hamiltonian (A2):

$$t\alpha_s \to t(1-\beta u_{ss})\alpha_s + t\beta\sum_{s'\neq s} u_{ss'}\alpha_{s'}, \tag{A9a}$$

$$r \to r_s = r(1-\beta u_{ss}). \tag{A9b}$$

The tensor u_{ij} is the strain tensor. We will make the approximation of setting all the Gruneisen parameters β to be equal. After expanding first around the Weyl points and applying these changes in (A2) we can split the new Hamiltonian into $H_0 + H[u]$:

$$H[u] = -\beta v\tau\lambda_3\sum_k u_{33}c^+_{\boldsymbol{k}}\alpha_3 c_{\boldsymbol{k}} + \beta v\tau\lambda_3\sum_{s\neq 3} u_{3s}c^+_{\boldsymbol{k}}\alpha_s c_{\boldsymbol{k}} + r\beta\sum_{\boldsymbol{k}} Tr[u]c^+_{\boldsymbol{k}}\hat{\beta}c_{\boldsymbol{k}}. \tag{A10}$$

Remembering the expression (A4) relating the high energy sector to the low energy sector, we can evaluate the elements of the type $c^+_{\boldsymbol{k}}\alpha_s c_{\boldsymbol{k}}$ keeping the lowest order in a $1/(m+b_3)$ expansion:

$$c^+_{\boldsymbol{k}}\alpha_3 c_{\boldsymbol{k}} \simeq \phi^+_{\boldsymbol{k}}\sigma_3\psi_{\boldsymbol{k}} + \psi^+_{\boldsymbol{k}}\sigma_3\phi_{\boldsymbol{k}} = -\frac{2}{m+b_3}\psi^+_{\boldsymbol{k}}(\tau v\lambda_3\sigma_3 + b_0\sigma_0)\psi_{\boldsymbol{k}}, \tag{A11a}$$

$$c^+_{\boldsymbol{k}}\alpha_s c_{\boldsymbol{k}} \simeq \psi^+_{\boldsymbol{k}}\sigma_s\psi_{\boldsymbol{k}}, \tag{A11b}$$

$$c^+_{\boldsymbol{k}}\hat{\beta}c_{\boldsymbol{k}} \simeq -\psi^+_{\boldsymbol{k}}\sigma_3\psi_{\boldsymbol{k}}. \tag{A11c}$$

With these expressions, we the have

$$\begin{aligned} H[u] = &\sum_k\left(2\tau b_0\beta\frac{v\lambda_3}{m+b_3}u_{33}\right)\psi^+_{\boldsymbol{k}}\sigma_0\psi_{\boldsymbol{k}} + \sum_{k,s=1,2}\left(\tau\beta v\lambda_3 u_{3s}\right)\psi^+_{\boldsymbol{k}}\sigma_s\psi_{\boldsymbol{k}} + \\ &+\sum_k\left(2\beta\frac{v^2\lambda_3^2}{m+b_3}u_{33} - \beta r Tr[u]\right)\psi^+_{\boldsymbol{k}}\sigma_3\psi_{\boldsymbol{k}}, \end{aligned} \tag{A12}$$

from which we can read the components of the elastic vector field:

$$A^{el}_0 = \tau b_0\beta\frac{2v\lambda_3}{m+b_3}u_{33}, \tag{A13a}$$

$$A^{el}_1 = \tau\beta v\lambda_3 u_{31}, \tag{A13b}$$

$$A^{el}_2 = \tau\beta v\lambda_3 u_{32}, \tag{A13c}$$

$$A^{el}_3 = 2\beta\frac{v^2\lambda_3^2}{m+b_3}u_{33} - \beta r Tr[u]. \tag{A13d}$$

The novelty now is that, because the presence of the term b_0 in the original hamiltonian, a chiral zeroth component of the elastic vector field appears.

[1] Bertlmann, R. A. *Anomalies in quantum field theory* (Oxford, UK: Clarendon, 1996).

[2] Kharzeev, D. & Zhitnitsky, A. Charge separation induced

by p-odd bubbles in QCD matter. *Nucl. Phys. A* **797**, 67 (2007).

[3] Kharzeev, D., McLerran, L. D. & Warringa, H. J. The effects of topological charge change in heavy ion collisions: Event by event P and CP violation. *Nucl. Phys. A* **803**, 227 (2008).

[4] Fukushima, K., Kharzeev, D. & Warringa, H. J. The chiral magnetic effect. *Phys. Rev D* **78**, 074033 (2008).

[5] Başar, G. m. c., Kharzeev, D. E. & Yee, H.-U. Triangle anomaly in Weyl semimetals. *Phys. Rev. B* **89**, 035142 (2014).

[6] Li, Q., Kharzeev, D. *et al.* Chiral magnetic effect in $ZrTe_5$. *Nat. Phys.* **10**, 3648 (2016).

[7] Xu, S. Y. *et al.* Observation of fermi arc surface states in a topological metal: A new type of 2d electron gas beyond Z_2 topological insulators. *Science* **347**, 294 (2015).

[8] Xu, S. Y. *et al.* Discovery of a Weyl fermion state with Fermi arcs in niobium arsenide. *Nat. Phys.* **11**, 748 (2015).

[9] Lv, B. Q. *et al.* Experimental discovery of Weyl semimetal TaAs. *Phys. Rev. X* **5**, 031013 (2015).

[10] Grushin, A. G. Consequences of a condensed matter realization of lorentz-violating qed in Weyl semi-metals. *Phys. Rev. D* **86**, 045001 (2012).

[11] Vazifeh, M. M. & Franz, M. Electromagnetic response of Weyl semimetals. *Phys. Rev. Lett.* **111**, 027201 (2013).

[12] Gynther, A., Landsteiner, K., Pena-Benitez, F. & Rebhan, A. Holographic anomalous conductivities and the chiral magnetic effect. *JHEP* **1102**, 110 (2011). arXiv:1005.2587.

[13] Li, C. *et al.* Giant negative magnetoresistance induced by the chiral anomaly in individual Cd3As2 nanowires. *Nat. Comm.* **6**, 10137 (2015).

[14] Zhang, C. *et al.* Signatures of the Adler Bell Jackiw chiral anomaly in a Weyl fermion semimetal. *Nat. Comm.* **7**, 10735 (2016).

[15] Li, H., He, H. *et al.* Negative magnetoresistance in dirac semimetal Cd_3As_2. *Nat. Comm.* **7**, 10301 (2016).

[16] Shekhar, C. *et al.* Extremely large magnetoresistance and ultrahigh mobility in the topological Weyl semimetal candidate NbP. *Nat. Phys.* **11**, 645 (2015).

[17] Cortijo, A., Ferreiros, Y., Landsteiner, K. & Vozmediano, M. A. H. Elastic gauge fields in Weyl semimetals. *Phys. Rev. Lett.* **115** (2015).

[18] Cortijo, A. & Zubkov, M. A. Emergent gravity in the cubic tight-binding model of Weyl semimetal in the presence of elastic deformations. *Annals of Physics* **366**, 45 – 56 (2016).

[19] Shapourian, H., Hughes, T. L. & Ryu, S. The viscoelastic response of topological tight-binding models in 2d and 3d. *Phys. Rev. B* **92**, 165131 (2015).

[20] Mañes, J. L., de Juan, F., Sturla, M. & Vozmediano, M. A. H. Generalized effective hamiltonian for graphene under nonuniform strain. *Phys. Rev. B* **88**, 155405 (2013).

[21] Xiong, J. *et al.* Evidence for the chiral anomaly in the dirac semimetal Na_3Bi. *Science* **350**, 413 (2015).

[22] Behrends, J., Grushin, A. G., Ojanen, T. & Bardarson, J. H. Visualizing the chiral anomaly in dirac and weyl semimetals with photoemission spectroscopy. *Phys. Rev. B* **93**, 075114 (2016).

[23] The CME will occur for any value of the magnetic field, irrespective of how big it is compared with other scales of the problem, as the thermal length or the wavelengh at the Fermi level. We have chosen the value of 1T for concreteness.

[24] Sekine, A. & Nomura, K. Chiral magnetic effect and anomalous hall effect in antiferromagnetic insulators with spin-orbit coupling. *Phys. Rev. Lett.* **116**, 096401 (2016).

[25] Baireuther, P., Hutasoit, J. A., Tworzydo, J. & Beenakker, C. W. J. Scattering theory of the chiral magnetic effect in a weyl semimetal: interplay of bulk weyl cones and surface fermi arcs. *New Journal of Physics* **18**, 045009 (2016).

[26] Borisenko, S. *et al.* Time-Reversal Symmetry Breaking Type-II Weyl State in YbMnBi2. *ArXiv e-prints* (2015). 1507.04847.

[27] Liu, J. Y. *et al.* Discovery of a topological semimetal phase coexisting with ferromagnetic behavior in Sr1-yMnSb2 (y˜0.08). *ArXiv e-prints* (2015). 1507.07978.

[28] Chang, G. *et al.* Theoretical prediction of magnetic and noncentrosymmetric Weyl fermion semimetal states in the R-Al-X family of compounds (R=rare earth, Al=aluminium, X=Si, Ge). *ArXiv e-prints* (2016). 1604.02124.

[29] Wang, Z. *et al.* Time-Reversal Breaking Weyl Fermions In Magnetic Heuslers. *ArXiv e-prints* (2016). 1603.00479.

[30] Hosur, P. & Qi, X. Recent developments in transport phenomena in Weyl semimetals. *Comptes Rendus Physique* **14**, 857 (2013).

[31] Chernodub, M. N., Cortijo, A., Grushin, A. G., Landsteiner, K. & Vozmediano, M. A. H. Condensed matter realization of the axial magnetic effect. *Phys. Rev. B* **89**, 081407 (2014).

[32] Burkov, A. A. Chiral anomaly and transport in Weyl metals. *Journal of Physics: Condensed Matter* **27**, 113201 (2015).

[33] Bzdušek, T. c. v., Rüegg, A. & Sigrist, M. Weyl semimetal from spontaneous inversion symmetry breaking in pyrochlore oxides. *Phys. Rev. B* **91**, 165105 (2015).

[34] Ruan, J. *et al.* Symmetry-protected ideal weyl semimetal in $HgTe$-class materials. *Nat. Comm.* **7**, 11136 (2016).

[35] Volovik, G. E. Topological Lifshitz transitions. *ArXiv e-prints* (2016). 1606.08318.

[36] We thank G. Volovik for suggesting this possibility.

[37] Pikulin, D., Chen, A. & Franz, M. Chiral anomaly from strain-induced gauge fields in dirac and weyl semimetals. *arXiv:1607.01810* (2016).

[38] Grushin, A. G., Venderbos, J. W. F., Vishwanath, A. & Ilan, R. Inhomogeneous weyl and dirac semimetals: Transport in axial magnetic fields and fermi arc surface states from pseudo landau levels. *arXiv:1607.04268* (2016).